https://doi.org/10.5194/egusphere-2022-145
Preprint. Discussion started: 11 April 2022

Development of a broadband cavity-enhanced absorption spectrometer for simultaneous measurements of ambient NO_3, NO_2, and H_2O

Woohui Nam[1], Changmin Cho[1], Begie Perdigones[1], Tae Siek Rhee[2], and Kyung-Eun Min[1]

[1]School of Earth Science and Environmental Engineering, Gwangju Institute of Science and Technology (GIST),123 Cheomdangwagi-ro, Buk-gu, Gwangju 61005, South Korea
[2]Korea Polar Research Institute, 26 Songdomirae-ro, Yeonsu-gu, Incheon 21990, South Korea

Correspondence to: Kyung-Eun Min (kemin@gist.ac.kr)

Abstract. We describe the characteristics and performances of our newly built broadband cavity-enhanced absorption spectrometer for measurements of nitrate radical (NO_3), nitrogen dioxide (NO_2), and water vapor (H_2O). A customized vibration-resistance cavity layout incorporated with N_2 purging on high-reflection mirror surfaces was implemented with a red light-emitting diode (LED) as a light source. In general, this system achieved over 40 km (up to 101.5 km) of effective light path length at 662 nm from a 0.52 m long cavity. For the accurate NO_3 measurement, the measured absorption spectrum of H_2O was used for simultaneous concentration retrievals with the other species, instead of being treated as interferences to be removed or corrected prior to NO_3 detection. Synthesized N_2O_5 crystals under atmospheric pressure were used for performance tests of linear response and transmission efficiency. From the standard injection experiments of NO_3, NO_2, and H_2O, high linearities were observed ($R^2 \geq 0.9918$). The total NO_3 transmission efficiency through the system was determined to be 81.2 % (±2.9, 1σ) within the residence time of 2.59 seconds. The precisions (1σ) of NO_3, NO_2, and H_2O in 1 Hz measurement from a single pixel on the CCD were 1.41 pptv, 6.92 ppbv, and 35.0 ppmv with uncertainties of 10.8, 5.2, and ≥20.5 %, respectively, mainly from the errors in literature absorption cross-sections. The instrument was successfully deployed aboard the Korean icebreaker R/V *Araon* for an expedition conducted in remote marine boundary layer in the Arctic Ocean during the summer of 2021.

1 Introduction

The nitrate radical (NO_3) has drawn considerable attention due to its significant influence on nocturnal nitrogen oxide chemistry after the first observation in the troposphere (Noxon et al., 1980; Platt et al., 1980; Brown and Stutz, 2012). NO_3 is mainly produced from the oxidation of nitrogen dioxide (NO_2) by ozone (O_3, R1) and is in thermal equilibrium with dinitrogen pentoxide (N_2O_5) from its further combination reaction with NO_2 (R2).

The role of NO_3 as an oxidant especially for the unsaturated volatile organic compounds (VOCs) becomes more critical at night not only because of its extremely low abundance due to the losses by rapid photolysis (R3; Stark et al., 2007) and reaction with NO (R4) but also because of the negligible amount of photochemically induced hydroxyl radical. Particularly, alkenes from biogenic sources with more than two double bonds (e.g., isoprene and terpenes; Winer et al., 1984; Ng et al., 2017) and reduced sulfur compounds like dimethylsulfide (DMS; Allan et al., 2000) are susceptible to be oxidized by NO_3 (R5).

$$NO_2 + O_3 \rightarrow NO_3 + O_2 \tag{R1}$$

$$NO_3 + NO_2 + M \leftrightarrow N_2O_5 + M \tag{R2}$$

$$NO_3 + h\upsilon \rightarrow NO_2 + O(^3P)\ (< 587\ \mathrm{nm})$$

$$NO_3 + h\upsilon \rightarrow NO + O_2\ (< 714\ \mathrm{nm}) \tag{R3}$$

$$NO_3 + NO \rightarrow 2NO_2 \tag{R4}$$

$$NO_3 + \text{alkenes, aromatics, DMS} \rightarrow \text{product} \tag{R5}$$

$$N_2O_{5(g)} + (H_2O_{(aq)}\ \text{and/or}\ Cl^-_{(aq)}) \rightarrow (2-\varphi)NO^-_{3(aq)} + \varphi ClNO_{2(g)},\ (0 \le \varphi \le 1) \tag{R6}$$

As shown in reaction (R6), reservoir species of NO_3, N_2O_5, can undergo heterogeneous reaction to form gaseous nitryl chloride ($ClNO_2$) and/or aqueous nitrate (Roberts et al., 2008). This uptake on aerosol can act as a dominant nitrate formation path under haze events (Chang et al., 2018; McDuffie et al., 2019; Lin et al., 2020; Liu et al., 2020). Meanwhile, $ClNO_2$ can be photolyzed to NO_2 and Cl radical after following sunrise; consequently, it does not only conserve NO_x (=NO + NO_2) but also accelerate oxidation speed by adding the Cl radical into the atmosphere (Osthoff et al., 2008; Le Breton et al., 2018).

In addition, the important roles of daytime NO_3 and N_2O_5 have been reported in terms of their contributions to VOC oxidation and aerosol evolution (Geyer, 2003; Brown et al., 2005; Osthoff et al., 2006; Wang et al., 2014; Brown et al., 2016; Brown et al., 2017; Wang et al., 2020; Foulds et al., 2021). Brown et al. (2017) observed non-negligible amount of N_2O_5 (up to 35 pptv) during the daytime under high NO_x conditions and Foulds et al. (2021) found competitive NO_3 loss by VOC oxidation with photolysis, even in daytime. These findings indicate that the impacts of NO_3-driven chemistry is not limited to nighttime.

Because of high reactivity, thus short lifetime, and low mixing ratio (a few to several pptv), observation of the ambient NO_3 is challenging. To our best knowledge, no commercial instruments are available at present, and only a few in situ measurement techniques have been used. Systems based on laser-induced fluorescence (LIF; Wood et al., 2003; Matsumoto et al., 2005) and matrix isolation electron spin resonance (MIESR; Mihelcic et al., 1993) had been reported. However, most of the contemporary instruments in active use even in intercomparison work (Dorn et al., 2013) are based on absorption spectroscopic techniques capturing the strong $B^2E'\text{-}X^2A'_2$ electronic transition of NO_3 at 662 nm (Yokelson et al., 1994). Differential optical absorption spectroscopy (DOAS), characterized with a long physical path length, has been widely used for several decades (Platt et al., 1980; Heintz et al., 1996; Allan et al., 1999; Geyer et al., 2001b; McLaren et al., 2004; Stutz, 2004; Vrekoussis et al., 2004; Li

https://doi.org/10.5194/egusphere-2022-145
Preprint. Discussion started: 11 April 2022

et al., 2007; Sommariva et al., 2007; Asaf et al., 2009; Wang et al., 2013; Lu et al., 2016). Meanwhile, more compact instruments with an optical cavity have been recently developed for NO_3 measurements; cavity ring-down spectroscopy (CRDS; King et al., 2000; Brown et al., 2001; Simpson, 2003; Ayers et al., 2005; Nakayama et al., 2008; Schuster et al., 2009; Flemmer and Ham, 2012; Hu et al., 2014; Wang et al., 2015; Li et al., 2018; Wu et al., 2020) and cavity-enhanced absorption spectroscopy (CEAS) are the most representative techniques. In particular, CEAS instruments with broadband light sources for NO_3 measurement were developed for field (Langridge et al., 2008; Varma et al., 2009; Kennedy et al., 2011; Wang et al., 2017; Suhail et al., 2019; Wang and Lu, 2019) and laboratory studies (Venables et al., 2006; Wu et al., 2014; Fouqueau et al., 2020) with advantages of capability for simultaneous measurements of multiple species and applicability of cheap light sources (e.g., light-emitting diode (LED), arc Xe lamp, and supercontinuum radiation source).

One of the main difficulties for accurate NO_3 measurement by CEAS is H_2O treatment. Due to the strong but narrow absorption by H_2O around 660nm (Ball and Jones, 2003), the contribution of H_2O on light extinction needs to be well characterized. Several methods such as look-up table (Langridge et al., 2008; Varma et al., 2009; Suhail et al., 2019), iterative calculation (Kennedy et al., 2011), and frequent NO_3 zeroing via NO titration (Wang et al., 2017) were adopted to overcome this issue.

Based on the capability of species-specific absorption cross-section measurements by CEAS (Axson et al., 2011; Chen and Venables, 2011; Young et al., 2011; Kahan et al., 2012; Sheps, 2013; Thalman and Volkamer, 2013; Young et al., 2014; Prakash et al., 2018; He et al., 2021; Wang et al., 2022), we suggest a new approach using measured H_2O spectrum for simultaneous quantification of NO_3, NO_2, and H_2O which is simple and efficient enough for atmospheric application. Through this manuscript, we present not only our newly built broadband cavity-enhanced absorption spectrometer (BBCEAS) with detailed descriptions of design and performances but also the linearity test results with H_2O in atmospherically relevant ranges. Moreover, we also show the results of the shipborne measurement of NO_3 in the Arctic Ocean, indicating successful performance of the instrument in field application.

2 Instrumental setup

BBCEAS is a sensitive technique to directly measure the abundance of target species and/or its optical extinction properties, introduced by Fiedler et al. (2003). Details on the working principle can be found in Ball and Jones (2003) as well as Gagliardi and Loock (2014). Briefly, this technique is based on the measurement of light extinctions in a relatively broad wavelength range. System based on this method basically consists of a broadband light source, a high-finesse optical cavity formed by a pair of high-reflection (HR) mirrors, and detector(s). The light from the source resonates inside the cavity and rapidly reaches a steady state with the wavelength-specific attenuated intensity through the loss processes of (1) transmission, diffraction, and absorption by HR mirrors, (2) scattering by particles and gases (i.e. Mie and Rayleigh scattering), and (3) absorption by sampled trace gases in the cavity. The transmitted light from the cavity is then detected by the spectrometer and charge-coupled device (CCD) or photodiode array to monitor the light extinction spectrum.

The schematic diagram of our single channel BBCEAS is shown in Figure 1. The material, dimensions, and design of the novel cage system on optical mounts for stable performance with respect to vibration and pressure changes during the field deployment were adopted from the glyoxal (CHOCHO) and nitrous acid (HONO) instrument described in Min et al. (2016). Detailed descriptions of the optical layout, flow system, and data acquisition system are described in the following section.

2.1 Optical layout

An LED (LZ1-10R202-0000, LedEngin, Germany) centered at 660 nm is used as a broadband light source and is mounted on a home-built module with copper plate, thermoelectric cooler, heatsink, XYZ translator (LP-1A-XYZ, Newport Corp., USA), and fan to control the position and temperature (20±0.1 ºC) precisely. The light from the LED is collimated by an off-axis parabolic mirror (50328AU, Newport Corp., USA) and enters the cavity. The HR mirrors (FiveNine Optics, USA) for high-finesse optical cavity are mounted at a distance of 51.5 cm occupied by a Teflon cell (1 in. outer diameter (o.d.), and 1 mm thickness). The light exiting the cavity is then focused by another parabolic mirror (50331AU, Newport Corp., USA), filtered through a colored band-pass filter (660±5 nm, FB-660-10, Thorlabs Inc., USA), and coupled to a fiber collimator (74-UV, Ocean Optics Inc., USA). The customized optic fiber (Seokwang Optical Co., Korea) with linearly assembled seven 200 µm diameter cores are aligned along the slit axis of the spectrometer (HRS-300MS-NI, Princeton Instruments Inc., USA).

Light is then transmitted to a diffraction grating (1200G/mm, 750nm blaze, 68 mm × 68 mm) and dispersed with respect to its wavelength. A CCD is used as a detector (PIXIS-2KX, Princeton Instruments Inc., USA) to monitor the spectra of the final transmitted light intensity, and is cooled to -70 ℃ to minimize the dark current. The wavelength coverage from 632 to 691 nm and the spectral resolution of 0.47 nm as full width at half maximum (FHWM) were calibrated with the narrow Ne emission lines (NE-2, Ocean Optics Inc., USA).

The overall configuration of the optics is similar to the system described by Min et al. (2016); however, the main difference is that we have an independent cavity for individual channel rather than two channels sharing one parabolic mirror plate. This modification minimizes potential interferences of light leaking from the adjacent cell and provides convenience in operation and maintenance aspects (i.e. HR mirror cleaning and LED swapping).

2.2 Flow and data acquisition system

Air sample is drawn into perfluoroalkoxy alkenes (PFA) inlet tubing with a constant flow rate of 2.5 slpm (standard liter per minute) by a mass flow controller (Alicat Scientific, USA) and a scroll pump (IDP-3, Agilent Technologies Inc., USA). The design of the coaxial inlet following Min et al. (2016) is used to minimize the pressure change during the mirror reflectivity measurements and sampling cycles (see Sect. 3.1.1). On the downstream of the inlet, a 2µm polytetra-fluoroethylene (PTFE) membrane filter (R2PJ047, Pall Corporation, USA) is used to minimize the light extinction owing to Mie scattering by sampled aerosols inside the cavity as well as to prevent reflectivity degradation of HR mirrors. The air then passes through 1/16 in. inner diameter (i.d.) PFA tubing into the cavity to minimize NO_3 loss by shortening the residence time with the scheme of reduced pressure operation as in Fuchs et al. (2008). The temperature and pressure inside the cavity are measured at the outflow of the cell.

Another difference with the cavity system in Min et al. (2016) is the addition of purging system. As an active strategy to prevent sampled air contact on HR mirror surface, ultra-high purity (UHP) N_2 flows (> 99.999 %, 20 standard cubic centimeter per minute, sccm) are introduced on each side of the cavity mirrors via custom-designed PFA cell flanges with orifices (50µm, SS-1/8-Tube-50, Lenox Laser, USA). The effect of purge flow on the volume occupied by the air sample in the cavity was estimated as in Sect. 3.1.2.

Our instrument is operated and controlled automatically with the customized software programmed by LabView (National Instruments) for flow rates and temperatures of LED and CCD. The transmitted light spectra and other auxiliary data including temperatures, pressures, and flow rates for the extinction spectrum calculation are acquired via this program as well.

3 Characterization

From the spectrum of measured light extinction inside the cavity, $\alpha(\lambda)$, the number density (x_i) of species i can be calculated from the equation (1).

$$\alpha(\lambda) = \sum T_i \sigma_i(\lambda) x_i + \alpha_{Mie} + \alpha_{Rayleigh} = \left(\frac{1-R(\lambda)}{d_{eff}}\right)\left(\frac{I_{out,0}(\lambda)}{I_{out}(\lambda)} - 1\right) \tag{1}$$

Here, T_i is the transmission efficiency from the inlet to the cavity, σ_i corresponds to the absorption cross-section, R stands for mirror reflectivity, and d_{eff} is effective cavity length. The $\alpha_{Rayleigh}$ and α_{Mie} refer to the optical extinctions due to Rayleigh and Mie scattering, while we neglect α_{Mie} owing to the aerosol filter on the inlet airway. The intensities of light transmitted from the cavity with and without the absorbing species are symbolized as I_{out} and $I_{out,0}$, respectively. Here, we define $I_{out,0}$ as the light intensity when the cavity is filled with dry zero air (ZA) only. Thus, for the accurate quantification of x_i based on equation (1), not only the reference spectrum σ_i but also the instrumental parameters such as d_{eff}, R, $I_{out,0}$, and T_i should be characterized beforehand.

3.1 Determination of cavity parameters

3.1.1 Mirror reflectivity, $R(\lambda)$

$R(\lambda)$ can be derived from the well-known Rayleigh scattering differences in two species and we selected helium (He) and ZA as shown in equation (2). For our instrument, 2.75 slpm flow of He or ZA (99.999 % each, Daedeok Gas Co. Ltd.) is overflowed into coaxial inlet tubing so that 2.5 slpm flow is introduced into the cavity same as the flow rate of sample, while the rest of the flow is streamed towards the outside of the inlet to minimize the pressure change inside the cavity.

$$R(\lambda) = 1 - d\left[\frac{I_{ZA}(\lambda)\alpha_{Rayleigh,ZA}(\lambda) - I_{He}(\lambda)\alpha_{Rayleigh,He}(\lambda)}{I_{He}(\lambda) - I_{ZA}(\lambda)}\right] = 1 - \frac{d}{L_{Light}(\lambda)} \quad (2)$$

In equation (2), I_i refers to the transmitted spectral intensity filled with gas species i. L_{Light} is the theoretically calculated effective light path length under the assumption that light attenuation is solely driven by the mirror and the cavity length, d. The $\alpha_{Rayleigh,i}$ was calculated from the literature Rayleigh scattering cross-sections of N_2 (Bodhaine et al., 1999), O_2, and He (Shardanand and Rao, 1977) considering pressure and temperature changes.

Figure 2 shows the cavity characteristics such as the $I_{ZA}(\lambda)$, $I_{He}(\lambda)$, $R(\lambda)$, and $L_{Light}(\lambda)$ as examples acquired during the $T_{E,NO3}$ quantification experiments (described in Sect. 3.3.2). Although the difference of the transmitted light intensities between He and ZA injections was largest at near 662 nm (Figure 2 (a)), the wavelength corresponding to the highest $R(\lambda)$ value was shifted to 672.5 nm due to the incorporated wavelength-dependent characteristics of Rayleigh scattering and mirror reflectivity (Figure 2 (b)). L_{Light} exceeded 98 km (Figure 2 (c)) within the wavelength range for fitting (shaded in light red in Figure 2). Especially at 662 nm where NO_3 absorption peaks, R and L_{Light} were 99.9995 % and 101.5 km, which are superior to other reported ones from previous studies (Table 1 in Sect. 3.5). The uncertainty for $R(\lambda)$ estimation is 2.2 %, mainly from error in Rayleigh scattering spectrum of ZA (2%; Washenfelder et al., 2008) and rarely from the temperature and pressure measurements (0.7 and 0.5 %, respectively).

3.1.2 Effective cavity length, d_{eff}

The volume occupied by the sample in the cavity should be accurately evaluated. Due to the reduction in the sample volume by addition of the purge flow, the d_{eff} differs from both the cavity length defined by mirror separation (51.5 cm) and the physical displacement of sample in and out ports (47.5 cm). This parameter has been commonly quantified by the injections of known amounts of standard gas such as H_2O (Kennedy et al., 2011), O_3 (Dubé et al., 2006; Fuchs et al., 2008), and NO_2 (Schuster et al., 2009; Wang et al., 2017). In this study, we filled the cavity with 5 ppmv NO_2 standard (in N_2, Korea Research Institute of Standards and Science, KRISS) and compared the retrieved NO_2 number densities with and without the purge flow. From this experiment, we concluded that the purge volume takes 1.67 cm^3 in the cylindrical cell (1 in. o.d. and 1 mm thickness) and thus estimated d_{eff} as 50.28 cm with an uncertainty of 5.2 % (1 % from the standard gas, 2.9 % and 2.6 % from retrieval errors, and 3.2 % from σ_{NO2} reported by Bogumil et al. (2003)).

3.2 Retrieval of number density

3.2.1 Absorption cross-section, σ_i

Number density x_i is determined from the optimal fit of $\sigma_i(\lambda)$ on the light extinction spectrum, $\alpha(\lambda)$, within broad spectral ranges. For σ_{NO_3}, convolved spectrum of literature cross-section from Yokelson et al. (1994) was used because of its simple outstanding absorption features as shown in Figure 3. Its uncertainty was reported as 10 %.

Measured spectra were used for H_2O and NO_2 to compensate for the imperfections in line-shape determination. These could be originated from the astigmatic bias on CCD pixels and from the environmental changes (i.e. pressure and temperature) in instrumental operation conditions. In order to minimize the impacts of these accumulated errors on concentration retrievals, measured spectra were used in previous studies (Min et al., 2016; Liang et al., 2019; Barbero et al., 2020) based on the fact that the CEAS technique is widely used to characterize the wavelength-dependent light extinction properties of chemical species (Thalman and Volkamer, 2010; Axson et al., 2011; Chen and Venables, 2011; Young et al., 2011; Kahan et al., 2012; Sheps, 2013; Thalman and Volkamer, 2013; Young et al., 2014; Prakash et al., 2018; Jordan et al., 2019; He et al., 2021; Wang et al., 2022).

As mentioned before, the treatment of H_2O absorption features is crucial for accurate NO_3 measurement due to its strong but narrow absorption lines around 660 nm. To prevent this issue, the measured H_2O spectrum scaled with literature and relative humidity (RH) probe was used as σ_{H_2O}. H_2O was produced by flowing ZA through a deionized water bubbler at room temperature, while activated carbon denuder (6 mesh, Ecotech Pty Ltd., Australia) as well as Drierite filter (8 mesh, Thermo Fisher Scientific, USA) were installed on upstream of the bubbler to remove possible contaminants in ZA cylinder. An averaged H_2O spectrum for 15 minutes injection was scaled with the literature spectrum from HITRAN2020 database (Gordon et al., 2022) in the range of 659.28-671.94 nm and the humidity transmitter (HMT337, Vaisala, Finland, uncertainty : 1 %) data.

Due to the weak but complex absorption features of NO_2 in the fitting range, we measured the absorption spectrum produced from 3-minute injection of NO_2 standard gas (10 ppmv in N_2, uncertainty 1 %, KRISS) passing through a trap immersed in dry ice to ensure H_2O-free condition. The acquired spectrum was scaled to the literature one from Bogumil et al. (2003) for the range of 649.64–672.79 nm where the most apparent NO_2 absorption features exist with minimum fitting error.

Although the application of the measured spectra improves the fitting performance in general, the uncertainties of σ_{H_2O} and σ_{NO_2} inevitably increased (≥20.1% and 3.3%, respectively) compared to the literature's (≥20% and 3.2%) owing to the additional errors caused by fitting procedure (1.3 % and 0.036 %) and number density calculation (0.86 % for both). Note that we only provide the lower limit error in σ_{H_2O} propagated from the absorption line-by-line uncertainties in HITRAN2020 (≥20%).

3.2.2 Spectral fitting

The Levenberg-Marquardt least-squares fitting software, DOASIS (Kraus, 2006), was applied for the spectral fitting of the extinction spectrum between 659.28 and 671.94 nm. Fourth-order polynomial was applied to account for the optical drift and/or unaccounted extinctions such as absorption by ambient ozone. The reference spectra were allowed to be shifted within ±1.0 nm and squeezed freely for the σ_{NO_3} but the measured ones were set to share the degree of horizontal shift and squeeze together. Figure 4 shows an example of simultaneous retrievals of 5.45 pptv NO_3, 5.75 ppbv NO_2, and 5620 ppmv H_2O with polynomial and fit residual from the ambient measurement during the Arctic shipborne mission (acquired at the open ocean on 26 August 2021, 17:11:41 UTC described in Sect. 4) with 2 seconds integration time.

3.3 NO_3 wall loss evaluation

Even though CEAS is able to measure the target species without concentration calibration using chemical standards in regular operation, indeed, the loss of NO_3 along the airway needs to be evaluated. Many previous works carefully characterized transmission efficiency of NO_3 for their instruments (Aldener et al., 2006; Dubé et al., 2006; Fuchs et al., 2008; Schuster et al., 2009; Kennedy et al., 2011; Wagner et al., 2011; Hu et al., 2014; Wang et al., 2015; Sobanski et al., 2016; Wang et al., 2017; Li et al., 2018). In line with this, we conducted a series of NO_3 injection experiments with a custom-built NO_3 generation system.

3.3.1 NO_3 generation

NO_3 was delivered from the synthesized N_2O_5 crystal under atmospheric pressure with the home-built system (Figure 5). To produce gaseous N_2O_5 via reactions (R1) and (R2), 5 to 10 % of O_3 was generated by corona discharge (Nano 15, Absolute Systems Inc., Canada) of O_2 (300 sccm of 99.999 % O_2 in N_2, Daedeok Gas Co. Ltd.). NO_2 (2 % in N_2, Daedeok Gas Co. Ltd.) was added in two different positions (500 and 200 sccm, respectively) into a quartz reactor (5 cm i.d. and 50 cm length) for efficient production of N_2O_5 crystals. To minimize HNO_3 formation in the reactor, any H_2O which can be present in the gas supplies as well as on all surfaces in the generation system was removed by heating the reactor (up to 120 °C) before the injection and by applying dry ice traps in front of the reactor during the synthesis. After the synthesis, additional O_3 was introduced on white N_2O_5 crystals to flush out the remaining HNO_3 for at least 30 minutes. The crystals were used immediately or trapped with dry ice and stored at -78 °C for later use.

Sub-ppbv to a few tens ppbv of NO_3 was produced by thermal equilibrium with the sublimated N_2O_5 introduced with a small flow of dry ZA (15 - 40 sccm) as a carrier gas passing the trap. Unlike previous studies (Fuchs et al., 2008; Kennedy et al., 2011; Odame-Ankrah and Osthoff, 2011; Wang et al., 2015; Wu et al., 2020), we did not provide any additional heat to shift the equilibrium towards NO_3 because the amount of NO_3 through this method was large enough to cover the ranges of typical atmospheric NO_3 mixing ratios in urban night conditions.

3.3.2 NO_3 transmission efficiency, $\boldsymbol{T_{NO_3}}$

NO_3 losses (T_{NO_3}) of individual parts along the airway before the detection region (i.e. overflow inlet, filter, and cavity cell) were quantified via continuous injection (at least 5 minutes) of the synthesized NO_3 under dark condition. Differences in NO_3 concentrations with and without each part of the flow system were acquired by periodic switching between two conditions under the same residence time using a three-way solenoid valve. In order to determine the effect of NO_3 loss on the aerosol-accumulated filter, filters with total ambient suspended particle loadings of 203, 335, and 1010 μg·cm^{-3} were compared with a clean one.

Figure 6 presents the results of the T_{NO_3} experiments for each of the test components with relative NO_3 concentration changes (concentrations in each step are normalized by the maximum value for every experiment resulting ranges from 745 pptv to 169 ppbv) since slow but steady increase in NO_3 concentrations was observed for all the experiments. We presumed that this drift may have been mainly due to the changes in temperature in dry ice bath where N_2O_5 crystals were placed and/or the variations in contact of ZA with the crystal surface. The comparisons of the retrieved NO_3 with and without each test part were achieved after reflecting the changes in slow increase by linear interpolations for the concentrations acquired in the same condition (shown as light red and gray dashed lines in Figure 6).

The T_{NO_3} of individual parts are 98.9 (±1.9, 1σ), 88.1 (±2.6) and 93.1 (±0.3) % for coaxial overflow inlet (residence time < 0.03 seconds), cavity cell (residence time < 2.59 seconds), and filter assembly (clean case), respectively. The largest loss was observed within the cavity cell due to its relatively large surface area and long residence time compared to the other parts of the flow system. The quantified NO_3 loss on a clean filter surface (93.1±0.3 %) was similar to previous studies (85 (±10, 1σ) % on Aldener et al. (2006); 93 (±2) % on Dubé et al. (2006); 95 (±2) % on Fuchs et al. (2008); 84.8 (±10) % on Schuster et al. (2009); 92 (±3) % on Wang et al. (2015)). Interestingly, the used filters showed no significant differences compared to the clean one regardless of the ambient aerosol loadings within the experimental range (93.1 (±0.1, 1σ), 92.9 (±0.1), and 92.7 (±2.0) % for 203, 335 and 1010 μg·cm^{-3}, respectively) which agree with Fuchs et al. (2008) and Zhou et al. (2018) . From the results, total T_{NO_3} was quantified to be 81.2 % (±2.9, 1σ) under 2.5 slpm sampling condition.

3.4 Linearity tests

To test the linearity in signal response against the concentrations of species, standard injection experiments were performed. Multiple mixing ratios were achieved by regulating the degree of dilutions in synthesized N_2O_5 crystals, NO_2 standard (5 ppmv in N_2, KRISS, uncertainty: 1 %), and deionized water from the bubbler. As described in section 3.3.2, a slow and steady increase in NO_3 was observed, varying from 746 to 1045 pptv under the constant dilution ratio of 1:150 from beginning to end of the experiment. For tracking this drift in NO_3 standard, we alternated various dilution conditions with the base one (dilution ratio set as 1:150, shown in black markers in Figure 7 (a, b)) and applied the linear interpolation of retrieved NO_3 concentrations in those conditions.

Figure 7 shows the results of standard additions with respect to the elapsed time (left) and other independent concentration evaluation parameters (right; i.e. dilution ratio for NO_3, nominal concentration for NO_2, and independent RH measurement for H_2O). Dashed lines in Figure 7 (b, d, and f) represent the correlations considering their errors (uncertainty of the parameter on x-axis and 1σ variabilities in measurements on y-axis). Dilution ratio of NO_3 is calculated from the flow rate of ZA passed over the source divided by the total flow rate and NO_2 standard concentration is from nominal concentration on manufacturer's specification with dilution ratio. RH was measured at the inlet tip by the humidity transmitter (HMT337, Vaisala, Finland) with the measurement uncertainty of 1 %.

All species show good linearities (R^2 of 0.9918, 0.9985, and 0.9980 for NO_3, NO_2, and H_2O, respectively) indicating the feasibility of atmospheric applications on those species. For NO_2, the intercept of 0.12 ppbv is insignificant considering the limit of detection (will be discussed in Sect. 3.5). However, the intercept of -143 pptv in NO_3 is larger than the observed precision of the instrument (Sect. 3.5). It is likely due to the variabilities in our NO_3 source and/or the variations in offsets of slow drift correction since the source has the minimum flow rate requirements to operate. In addition, the negligible retrieved NO_3 (0.077±1.46 pptv, average and 1σ for 1s integration data) during the N_2 injection experiment, described in Sect. 3.5, can be used as an alternative to evaluate the zero offsets.

For H_2O, 84 ppmv of the intercept was found which is in a similar order of magnitude as with its precision (35 ppmv for 1 s integration time). This may be attributable to not only the random noise in detection but also the zero offset in the humidity transmitter (uncertainty: 1%). From this high linear response of our instrument in H_2O measurements in varying atmospheric relevant ranges, we would like to emphasize that the difficulties in retrieval in NO_3 measurement due to H_2O can be alleviated by simultaneous measurement with instrument-specific absorption spectrum of H_2O without any pre-treatment to remove it.

3.5 Precision and accuracy

Allan deviation method is often used to determine the instrumental precision and the optimal integration time (Allan, 1966; Werle et al., 1993). Minimum detectable extinction for each pixel of the CCD was extracted from 1 hour injection of UHP N_2 with 1 second integration time. Figure 8 (a) shows the time series of the light extinction (α_{N_2}) at 662 nm (corresponding to 1024th pixel) where NO_3 absorbance peaks. α_{N_2} shows no significant time-dependent changes and it deviates around zero, which is likely dominated by white noise. Figure 8 (b) shows the Allan deviation for the single pixel corresponding to 662 nm. Up to around 900 s, 1σ precision generally follows the statistical limit which implies that there are no significant integration time-dependent systematic errors up to 900 s but it starts to gradually diverge after that, which is likely due to the instrumental drifts such as changes in conditions of the light source and/or CCD.

By only using the corresponding absorption cross-section on that single pixel, the detection limits for NO_3, NO_2, and H_2O are determined to be 1.41 (0.15) pptv, 6.92 (0.73) ppbv, and 35.0 (3.69) ppmv, respectively, for 1 (60) second(s) averaging under 1 atm and 25 ℃ condition, by following Fouqueau et al. (2020). However, one should note that the spectral retrievals through the optimized fitting algorithm are likely to produce even lower detection limits than those from the single pixel because this method relies on the absorption features on broad wavelength ranges among hundreds of pixels.

Measurement uncertainties (1σ) for NO_3, NO_2, and H_2O are calculated to be 10.8, 5.2, and ≥20.5 %, respectively, by Gaussian propagation of the errors in absorption cross-section (NO_3: 10 %, NO_2: 3.3 %, and H_2O: ≥20.1 %), effective cavity length (3.4 %), and HR mirror reflectivity (2.2 %). Note that the fitting errors are not included here because the mathematical error varies with target species abundance. If there are strong signatures of target species in the measurement, fitting errors are negligible. However, for the extremely low abundance condition, the absorption features of target species weaken and thus the fit result likely end up to produce physically meaningless number with large error because of the limitations in numerical fitting algorithms. Hence, when the fitting error outweighs the abundance of target species, interpretations should be limited.

Table 1 summarized the cavity characteristics and performances of the existing BBCEASs for NO_3 measurement. Our instrument has the longest effective light path length even though the mirror displacement is relatively short. Since this system is able to observe the optical extinctions in the order of 10^{-10} cm^{-1} within 1 second time resolution, we can conclude that our instrument is adequate for measuring ambient NO_3 abundances in terms of sensitivity aspect. The capabilities of operation and utilization for actual application are described in the following section.

4 Field deployment

In order to demonstrate the feasibility of the instrument in field measurements, we deployed our system on the Korean ice breaker R/V *Araon* and operated from late July to early September in 2021 for the expedition in Chukchi Sea and East Siberian Sea of Arctic Ocean (Figure 9 (a)). The instrument was housed in a seatainer placed on the compass deck (29 m above sea level). Inlet was installed on the window and covered by the weatherproof-designed stainless steel pipe (7.5 cm o.d.). To minimize the loss of NO_3 along the sampling line, air was subsampled from the center of main flow (1 in. o.d., 1 mm thickness, PFA tubing, 20 slpm). The profile of the main flow was maintained to be steady and laminar (Reynolds number ≅ 1230) by the blower (DB-200, Manseung Electric Co., Korea). Total length and residence time inside the main flow was kept to be as short as possible to minimize the loss. However, due to the physical limitation of the instrument placement in the seatainer, the length of subsampled PFA tubes was elongated (length: < 1 m, residence time: < 1.5 s) and the total transmission efficiency of NO_3 for this deployment was decreased by 65.1 % (±2.14 %, 1σ).

Aerosol filters were replaced by an integrated auto-filter changer (Dubé et al., 2006) only during the early and later stage of the mission near the coastal region of Northeast Asia for every three hours and manually changed with intervals of four to six hours in remote region since the demands for changing the filter were scarce due to the low aerosol loading in the Arctic region. The $R(\lambda)$ and $I_{out,0}(\lambda)$ were checked every two hours and instantaneously interpolated for real-time $\alpha(\lambda)$ calculation. During the campaign, R(at 662 nm) were varying in the range from 99.9985 % to 99.9989 %, which are lower than the best performances of the instrument in the laboratory, mainly due to the difference in proficiency and environment for cleaning

https://doi.org/10.5194/egusphere-2022-145
Preprint. Discussion started: 11 April 2022

optics but still high enough for ambient monitoring of NO_3. The negligible change in *R* is a direct evidence that our vibration-resistant design is robust despite the strong vibrations in the platform due to the sea ice breaking activities.

Figure 9 (b-d) shows the time series of H_2O, NO_2, and NO_3 (1 minute averaged), as well as O_3 monitored by the UV absorption instrument (49i, Thermo Fisher Scientific, USA), radiance (CNR4, Kipp & Zonen, Netherland) and production rate of NO_3, $P(NO_3)$, calculated as equation (3). For H_2O, our measurements were compared to the calculated values from the pressure (PTB110, Vaisala, Finland), relative humidity, and temperature (HMP155, Vaisala, Finland) data measured on mainmast of the icebreaker. Here we only show the selected period (23 August at 17:00 – 25 August at 15:10 in 2021 UTC) when the NO_3 signals were continuously observed well above the detection limit. H_2O mixing ratios measured by our instrument were ranged from 4160 to 6510 ppmv (mean of 5580 ppmv) and average (maximum) value(s) of NO_2 and NO_3 were 3.21 (23.9) ppbv and 2.53 (9.51) pptv, respectively. H_2O concentrations measured by both instruments were in good agreement considering the uncertainty of H_2O for our instrument (≥ 20.5 %).

$$P(NO_3) = k_{R1}\,[NO_2]\,[O_3] \qquad (3)$$

During the campaign, several fresh emissions from R/V *Araon* were observed, represented by sharp changes in O_3 and NO_2 as shown in Figure 9 (c) indicating that O_3 was titrated by NO and formed NO_2. These exhaust emissions lasted from a few minutes to several hours depending on the atmospheric conditions such as wind direction and atmospheric stability as well as movement of the vessel (i.e. sailing or anchoring in one place for marine survey).

$P(NO_3)$ was generally small but rose up to 0.66 ppbv hr^{-1} (mean of 0.21 ppbv hr^{-1}) depending on whether the sampled air masses were directly influenced by the ship plumes or not, but still lower than those observed in previous works during summertime; 0.31 ppbv hr^{-1} in rural areas (Geyer et al., 2001a) and 1.10 - 3.2 ppbv hr^{-1} in urban areas (Wang et al., 2013; Brown et al., 2017; Zhou et al., 2018) . Within the plume condition, maximum NO_3 increased up to 1.85 pptv even though there was sunlight at that time. The trend of NO_3 concentration was well-matched with $P(NO_3)$ for most of the period indicating the suitability of our instrument for ambient NO_3 measurements. Further analysis related with regional impacts of ship plume chemistry together with NO_3 oxidation assessment with observed VOCs and DMS would be interesting topics for future studies.

5 Conclusions

This paper describes our newly built cavity-enhanced absorption spectrometer for simultaneous measurements of ambient NO_3, NO_2, and H_2O from their absorption features in 659.28-671.94 nm. High performances in measurement capabilities and simplicity in maintaining and processing schemes were achieved by applying high-reflection mirrors (up to 99.9995 % at 662 nm), by integrating the mirror purge and cage system as well as by simultaneous quantification of H_2O using its measured spectrum. Generally, the light at 662 nm travels more than 40 km (up to 101.5 km) within the compact cavity cell (51.5 cm), which enables sensitive measurements of the target species. To overcome the difficulties in H_2O treatment for accurate NO_3 measurement, the measured absorption spectrum of H_2O was used and our instrument showed high linearity for varying atmospheric relevant ranges of H_2O. The transmission efficiency of NO_3 from the inlet tip to the detection region was evaluated as 81.2 (±2.9, 1σ) % within the residence time of 2.59 seconds from the prepared NO_3 addition experiments. Consequently, for NO_3, NO_2, and H_2O, the measurement accuracies and 1σ detection limit for 1 second integration time for a single pixel CCD were determined as 10.8 %, 4.7 %, and ≥20.5 % with 1.41 pptv, 6.92 ppbv, and 35.0 ppmv, respectively, which are sufficiently low for ambient applications.

The instrument was successfully deployed aboard the Korean ice breaker R/V *Araon* and captured not only the background condition of the atmosphere over the open ocean in the Arctic but also the highly structured features of the plumes which originated from the vessel exhaust during the campaign. In addition, the trend of NO_3 concentration was well-matched with the calculated $P(NO_3)$ which serves as a proof of the potential for active applications of this instrument in further studies not only in urban regions but also in pristine regions with any mobile platforms including aircraft and research vessel.

Data availability

The datasets used in this study are available upon request to the corresponding author, Kyung-Eun Min (kemin@gist.ac.kr).

Author contributions

WN and KEM contributed to designing and performing this study. TSR provided the data for O_3 and helped for the field deployment. WN and KEM wrote the manuscript with contributions from CC and BP. All co-authors revised the content of the original manuscript and approved the final version of the paper.

Competing interests

The authors declare that they have no conflict of interest.

Acknowledgements.

We thank all the crew members of R/V *Araon* for their support on the mission.

Financial support

This work was supported by the Korea Polar Research Institute (KOPRI) (PE21900) and by Korea Environment Industry & Technology Institute (KEITI) through Public Technology Program based on Environmental Policy Project, funded by Korea Ministry of Environment (MOE) (2019000160004).

References

Aldener, M., Brown, S. S., Stark, H., Williams, E. J., Lerner, B. M., Kuster, W. C., Goldan, P. D., Quinn, P. K., Bates, T. S., Fehsenfeld, F. C., and Ravishankara, A. R.: Reactivity and loss mechanisms of NO_3 and N_2O_5 in a polluted marine environment: Results from in situ measurements during New England Air Quality Study 2002, *J. Geophys. Res. Atmos.*, 111, n/a-n/a, doi:10.1029/2006jd007252, 2006.

Allan, B. J., Carslaw, N., Coe, H., Burgess, R. A., and Plane, J. M. C.: Observations of the nitrate radical in the marine boundary layer, *J. Atmos. Chem.*, 33, 129-154, doi:10.1023/a:1005917203307, 1999.

Allan, B. J., McFiggans, G., Plane, J. M. C., Coe, H., and McFadyen, G. G.: The nitrate radical in the remote marine boundary layer, *J. Geophys. Res. Atmos.*, 105, 24191-24204, doi:10.1029/2000jd900314, 2000.

Allan, D. W.: Statistics of atomic frequency standards, *Proc. IEEE*, 54, 221-230, doi:10.1109/proc.1966.4634, 1966.

Asaf, D., Pedersen, D., Matveev, V., Peleg, M., Kern, C., Zingler, J., Platt, U., and Luria, M.: Long-term measurements of NO_3 radical at a semiarid urban site: 1. Extreme concentration events and their oxidation capacity, *Environ. Sci. Technol.* , 43, 9117-9123, doi:10.1021/es900798b, 2009.

Axson, J. L., Washenfelder, R. A., Kahan, T. F., Young, C. J., Vaida, V., and Brown, S. S.: Absolute ozone absorption cross section in the Huggins Chappuis minimum (350–470 nm) at 296 K, *Atmos. Chem. Phys.*, 11, 11581-11590, doi:10.5194/acp-11-11581-2011, 2011.

Ayers, J. D., Apodaca, R. L., Simpson, W. R., and Baer, D. S.: Off-axis cavity ringdown spectroscopy: application to atmospheric nitrate radical detection, *Appl. Opt.*, 44, 7239-7242, doi:10.1364/AO.44.007239, 2005.

Ball, S. M., and Jones, R. L.: Broad-band cavity ring-down spectroscopy, *Chem. Rev.*, 103, 5239-5262, doi:10.1021/cr020523k, 2003.

Ball, S. M., Langridge, J. M., and Jones, R. L.: Broadband cavity enhanced absorption spectroscopy using light emitting diodes, *Chem. Phys. Lett.*, 398, 68-74, doi:10.1016/j.cplett.2004.08.144, 2004.

Barbero, A., Blouzon, C., Savarino, J., Caillon, N., Dommergue, A., and Grilli, R.: A compact incoherent broadband cavity-enhanced absorption spectrometer for trace detection of nitrogen oxides, iodine oxide and glyoxal at levels below parts per billion for field applications, *Atmos. Meas. Tech.*, 13, 4317-4331, doi:10.5194/amt-13-4317-2020, 2020.

Bodhaine, B. A., Wood, N. B., Dutton, E. G., and Slusser, J. R.: On Rayleigh optical depth calculations, *J. Atmos. Ocean. Tech.*, 16, 1854-1861, doi:10.1175/1520-0426(1999)016<1854:orodc>2.0.co;2, 1999.

Bogumil, K., Orphal, J., Homann, T., Voigt, S., Spietz, P., Fleischmann, O. C., Vogel, A., Hartmann, M., Kromminga, H., Bovensmann, H., Frerick, J., and Burrows, J. P.: Measurements of molecular absorption spectra with the SCIAMACHY pre-flight model: instrument characterization and reference data for atmospheric remote-sensing in the 230–2380 nm region, *J. Photochem. Photobiol. A* 157, 167-184, doi:10.1016/s1010-6030(03)00062-5, 2003.

Brown, S. S., Stark, H., Ciciora, S. J., and Ravishankara, A. R.: In-situ measurement of atmospheric NO_3 and N_2O_5 via cavity ring-down spectroscopy, *Geophys. Res. Lett.*, 28, 3227-3230, doi:10.1029/2001gl013303, 2001.

Brown, S. S., Osthoff, H. D., Stark, H., Dubé, W. P., Ryerson, T. B., Warneke, C., De Gouw, J. A., Wollny, A. G., Parrish, D. D., Fehsenfeld, F. C., and Ravishankara, A. R.: Aircraft observations of daytime NO_3 and N_2O_5 and their implications for tropospheric chemistry, *J. Photochem. Photobiol., A*, 176, 270-278, doi:10.1016/j.jphotochem.2005.10.004, 2005.

Brown, S. S., and Stutz, J.: Nighttime radical observations and chemistry, *Chem. Soc. Rev.*, 41, 6405, doi:10.1039/c2cs35181a, 2012.

Brown, S. S., Dubé, W. P., Tham, Y. J., Zha, Q., Xue, L., Poon, S., Wang, Z., Blake, D. R., Tsui, W., Parrish, D. D., and Wang, T.: Nighttime chemistry at a high altitude site above Hong Kong, *J. Geophys. Res. Atmos.*, 121, 2457-2475, doi:10.1002/2015jd024566, 2016.

Brown, S. S., An, H., Lee, M., Park, J.-H., Lee, S.-D., Fibiger, D. L., McDuffie, E. E., Dubé, W. P., Wagner, N. L., and Min, K.-E.: Cavity enhanced spectroscopy for measurement of nitrogen oxides in the Anthropocene: results from the Seoul tower during MAPS 2015, *Faraday Discuss.*, 200, 529-557, doi:10.1039/c7fd00001d, 2017.

Chang, Y., Zhang, Y., Tian, C., Zhang, S., Ma, X., Cao, F., Liu, X., Zhang, W., Kuhn, T., and Lehmann, M. F.: Nitrogen isotope fractionation during gas-to-particle conversion of NO_x to NO_3^- in the atmosphere – implications for isotope-based NO_x source apportionment, *Atmos. Chem. Phys.*, 18, 11647-11661, doi:10.5194/acp-18-11647-2018, 2018.

Chen, J., and Venables, D. S.: A broadband optical cavity spectrometer for measuring weak near-ultraviolet absorption spectra of gases, *Atmos. Meas. Tech.*, 4, 425-436, doi:10.5194/amt-4-425-2011, 2011.

Dorn, H. P., Apodaca, R. L., Ball, S. M., Brauers, T., Brown, S. S., Crowley, J. N., Dube, W. P., Fuchs, H., Haseler, R., Heitmann, U., Jones, R. L., Kiendler-Scharr, A., Labazan, I., Langridge, J. M., Meinen, J., Mentel, T. F., Platt, U., Pohler, D., Rohrer, F., Ruth, A. A., Schlosser, E., Schuster, G., Shillings, A. J. L., Simpson, W. R., Thieser, J., Tillmann, R., Varma, R., Venables, D. S., and Wahner, A.: Intercomparison of NO_3 radical detection instruments in the atmosphere simulation chamber SAPHIR, *Atmos. Meas. Tech.*, 6, 1111-1140, doi:10.5194/amt-6-1111-2013, 2013.

Dubé, W. P., Brown, S. S., Osthoff, H. D., Nunley, M. R., Ciciora, S. J., Paris, M. W., McLaughlin, R. J., and Ravishankara, A. R.: Aircraft instrument for simultaneous, in situ measurement of NO_3 and N_2O_5 via pulsed cavity ring-down spectroscopy, *Rev. Sci. Instrum.*, 77, doi:10.1063/1.2176058, 2006.

Fiedler, S. E., Hese, A., and Ruth, A. A.: Incoherent broad-band cavity-enhanced absorption spectroscopy, *Chem. Phys. Lett.*, 371, 284-294, doi:10.1016/s0009-2614(03)00263-x, 2003.

Flemmer, M. M., and Ham, J. E.: Cavity ring-down spectroscopy with an automated control feedback system for investigating nitrate radical surface chemistry reactions, *Rev. Sci. Instrum.*, 83, 085103, doi:10.1063/1.4739768, 2012.

Foulds, A., Khan, M. A. H., Bannan, T. J., Percival, C. J., Lowenberg, M. H., and Shallcross, D. E.: Abundance of NO_3 derived organo-nitrates and their importance in the atmosphere, *Atmosphere*, 12, 1381, doi:10.3390/atmos12111381, 2021.

Fouqueau, A., Cirtog, M., Cazaunau, M., Pangui, E., Zapf, P., Siour, G., Landsheere, X., Méjean, G., Romanini, D., and Picquet-Varrault, B.: Implementation of an incoherent broadband cavity-enhanced absorption spectroscopy technique in an atmospheric simulation chamber for in situ NO_3 monitoring: characterization and validation for kinetic studies, *Atmos. Meas. Tech.*, 13, 6311-6323, doi:10.5194/amt-13-6311-2020, 2020.

Fuchs, H., Dubé, W. P., Ciciora, S. J., and Brown, S. S.: Determination of inlet transmission and conversion efficiencies for in situ measurements of the nocturnal nitrogen oxides, NO_3, N_2O_5 and NO_2, via pulsed cavity ring-down spectroscopy, *Anal. Chem.*, 80, 6010-6017, doi:10.1021/ac8007253, 2008.

Gagliardi, G., and Loock, H. P.: Cavity-enhanced spectroscopy and sensing, Springer, 2014.

Geyer, A., Ackermann, R., Dubois, R., Lohrmann, B., Müller, T., and Platt, U.: Long-term observation of nitrate radicals in the continental boundary layer near Berlin, *Atmos. Environ.*, 35, 3619-3631, doi:10.1016/s1352-2310(00)00549-5, 2001a.

Geyer, A., Alicke, B., Konrad, S., Schmitz, T., Stutz, J., and Platt, U.: Chemistry and oxidation capacity of the nitrate radical in the continental boundary layer near Berlin, *J. Geophys. Res. Atmos.*, 106, 8013-8025, doi:10.1029/2000jd900681, 2001b.

Geyer, A., Alicke, B., Ackermann, R., Martinez, M., Harder, H., Brune, W., di Carlo, P., Williams, E., Jobson, T., and Hall, S.: Direct observations of daytime NO_3 : Implications for urban boundary layer chemistry, *J. Geophys. Res. Atmos.*, 108, doi:10.1029/2002jd002967, 2003.

Gordon, I. E., Rothman, L. S., Hargreaves, R. J., Hashemi, R., Karlovets, E. V., Skinner, F. M., Conway, E. K., Hill, C., Kochanov, R. V., Tan, Y., Wcisło, P., Finenko, A. A., Nelson, K., Bernath, P. F., Birk, M., Boudon, V., Campargue, A., Chance, K. V., Coustenis, A., Drouin, B. J., Flaud, J. M., Gamache, R. R., Hodges, J. T., Jacquemart, D., Mlawer, E. J., Nikitin, A. V., Perevalov, V. I., Rotger, M., Tennyson, J., Toon, G. C., Tran, H., Tyuterev, V. G., Adkins, E. M., Baker, A., Barbe, A., Canè, E., Császár, A. G., Dudaryonok, A., Egorov, O., Fleisher, A. J., Fleurbaey, H., Foltynowicz, A., Furtenbacher, T., Harrison, J. J., Hartmann, J. M., Horneman, V. M., Huang, X., Karman, T., Karns, J., Kassi, S., Kleiner, I., Kofman, V., Kwabia–Tchana, F., Lavrentieva, N. N., Lee, T. J., Long, D. A., Lukashevskaya, A. A., Lyulin, O. M., Makhnev, V. Y., Matt, W., Massie, S. T., Melosso, M., Mikhailenko, S. N., Mondelain, D., Müller, H. S. P., Naumenko, O. V., Perrin, A., Polyansky, O. L., Raddaoui, E., Raston, P. L., Reed, Z. D., Rey, M., Richard, C., Tóbiás, R., Sadiek, I., Schwenke, D. W., Starikova, E., Sung, K., Tamassia, F., Tashkun, S. A., Vander Auwera, J., Vasilenko, I. A., Vigasin, A. A., Villanueva, G. L., Vispoel, B., Wagner, G., Yachmenev, A., and Yurchenko, S. N.: The HITRAN2020 molecular spectroscopic database, *J. Quant. Spectrosc. Radiat. Transf.*, 277, 107949, doi:10.1016/j.jqsrt.2021.107949, 2022.

He, Q., Fang, Z., Shoshanim, O., Brown, S. S., and Rudich, Y.: Scattering and absorption cross sections of atmospheric gases in the ultraviolet–visible wavelength range (307–725 nm), *Atmos. Chem. Phys.*, 21, 14927-14940, doi:10.5194/acp-21-14927-2021, 2021.

Heintz, F., Platt, U., Flentje, H., and Dubois, R.: Long-term observation of nitrate radicals at the Tor Station, Kap Arkona (Rügen), *J. Geophys. Res. Atmos.*, 101, 22891-22910, doi:10.1029/96jd01549, 1996.

Hu, R.-Z., Wang, D., Xie, P.-H., Ling, L.-Y., Qin, M., Li, C.-X., and Liu, J.-G.: Diode laser cavity ring-down spectroscopy for atmospheric NO_3 radical measurement, *Acta. Phys. Sin.*, 63, 110707, doi:10.7498/aps.63.110707, 2014.

Jordan, N., Ye, C. Z., Ghosh, S., Washenfelder, R. A., Brown, S. S., and Osthoff, H. D.: A broadband cavity-enhanced spectrometer for atmospheric trace gas measurements and Rayleigh scattering cross sections in the cyan region (470–540 nm), *Atmos. Meas. Tech.*, 12, 1277-1293, doi:10.5194/amt-12-1277-2019, 2019.

Kahan, T. F., Washenfelder, R. A., Vaida, V., and Brown, S. S.: Cavity-enhanced measurements of hydrogen peroxide absorption cross sections from 353 to 410 nm, *J. Phys. Chem.*, 116, 5941-5947, doi:10.1021/jp2104616, 2012.

Kennedy, O. J., Ouyang, B., Langridge, J. M., Daniels, M. J. S., Bauguitte, S., Freshwater, R., McLeod, M. W., Ironmonger, C., Sendall, J., Norris, O., Nightingale, R., Ball, S. M., and Jones, R. L.: An aircraft based three channel broadband cavity enhanced absorption spectrometer for simultaneous measurements of NO_3, N_2O_5 and NO_2, *Atmos. Meas. Tech.*, 4, 1759-1776, doi:10.5194/amt-4-1759-2011, 2011.

King, M., Dick, E., and Simpson, W.: A new method for the atmospheric detection of the nitrate radical (NO_3), *Atmos. Environ.*, 34, 685-688, doi:10.1016/S1352-2310(99)00418-5, 2000.

Kraus, S.: DOASIS a framework design for DOAS, Shaker, 2006.

Langridge, J. M., Ball, S. M., Shillings, A. J. L., and Jones, R. L.: A broadband absorption spectrometer using light emitting diodes for ultrasensitive, in situ trace gas detection, *Rev. Sci. Instrum.*, 79, 123110, doi:10.1063/1.3046282, 2008.

Le Breton, M., Hallquist, Å. M., Pathak, R. K., Simpson, D., Wang, Y., Johansson, J., Zheng, J., Yang, Y., Shang, D., Wang, H., Liu, Q., Chan, C., Wang, T., Bannan, T. J., Priestley, M., Percival, C. J., Shallcross, D. E., Lu, K., Guo, S., Hu, M., and Hallquist, M.: Chlorine oxidation of VOCs at a semi-rural site in Beijing: significant chlorine liberation from $ClNO_2$ and subsequent gas- and particle-phase Cl–VOC production, *Atmos. Chem. Phys.*, 18, 13013-13030, doi:10.5194/acp-18-13013-2018, 2018.

Li, S., Liu, W., Xie, P., Li, A., Qin, M., and Dou, K.: Measurements of nighttime nitrate radical concentrations in the atmosphere by long-path differential optical absorption spectroscopy, *Adv. Atmos. Sci.*, 24, 875-880, doi:10.1007/s00376-007-0875-2, 2007.

Li, Z., Hu, R., Xie, P., Chen, H., Wu, S., Wang, F., Wang, Y., Ling, L., Liu, J., and Liu, W.: Development of a portable cavity ring down spectroscopy instrument for simultaneous, in situ measurement of NO_3 and N_2O_5, *Opt. Express*, 26, A433-A449, doi:10.1364/OE.26.00A433, 2018.

Liang, S., Qin, M., Xie, P., Duan, J., Fang, W., He, Y., Xu, J., Liu, J., Li, X., Tang, K., Meng, F., Ye, K., Liu, J., and Liu, W.: Development of an incoherent broadband cavity-enhanced absorption spectrometer for measurements of ambient glyoxal and NO_2 in a polluted urban environment, *Atmos. Meas. Tech.*, 12, 2499-2512, doi:10.5194/amt-12-2499-2019, 2019.

Lin, Y.-C., Zhang, Y.-L., Fan, M.-Y., and Bao, M.: Heterogeneous formation of particulate nitrate under ammonium-rich regimes during the high-$PM_{2.5}$ events in Nanjing, China, *Atmos. Chem. Phys.*, 20, 3999-4011, doi:10.5194/acp-20-3999-2020, 2020.

Liu, L., Bei, N., Hu, B., Wu, J., Liu, S., Li, X., Wang, R., Liu, Z., Shen, Z., and Li, G.: Wintertime nitrate formation pathways in the north China plain: Importance of N_2O_5 heterogeneous hydrolysis, *Environ. Pollut.*, 266, 115287, doi:10.1016/j.envpol.2020.115287, 2020.

Lu, X., Qin, M., Xie, P.-H., Duan, J., Fang, W., Ling, L.-Y., Shen, L.-L., Liu, J.-G., and Liu, W.-Q.: Measurements of atmospheric NO_3 radicals in Hefei using LED-based long path differential optical absorption spectroscopy, *Chin. Phys. B*, 25, 024210, doi:10.1088/1674-1056/25/2/024210, 2016.

Matsumoto, J., Kosugi, N., Imai, H., and Kajii, Y.: Development of a measurement system for nitrate radical and dinitrogen pentoxide using a thermal conversion/laser-induced fluorescence technique, *Rev. Sci. Instrum.*, 76, 064101, doi:10.1063/1.1927098, 2005.

McDuffie, E. E., Womack, C. C., Fibiger, D. L., Dube, W. P., Franchin, A., Middlebrook, A. M., Goldberger, L., Lee, B. H., Thornton, J. A., Moravek, A., Murphy, J. G., Baasandorj, M., and Brown, S. S.: On the contribution of nocturnal heterogeneous reactive nitrogen chemistry to particulate matter formation during wintertime pollution events in Northern Utah, *Atmos. Chem. Phys.*, 19, 9287-9308, doi:10.5194/acp-19-9287-2019, 2019.

McLaren, R., Salmon, R. A., Liggio, J., Hayden, K. L., Anlauf, K. G., and Leaitch, W. R.: Nighttime chemistry at a rural site in the Lower Fraser Valley, *Atmos. Environ.*, 38, 5837-5848, doi:10.1016/j.atmosenv.2004.03.074, 2004.

Mihelcic, D., Klemp, D., Müsgen, P., Pätz, H. W., and Volz-Thomas, A.: Simultaneous measurements of peroxy and nitrate radicals at Schauinsland, *J. Atmos. Chem.*, 16, 313-335, doi:10.1007/bf01032628, 1993.

Min, K. -E., Washenfelder, R. A., Dubé, W. P., Langford, A. O., Edwards, P. M., Zarzana, K. J., Stutz, J., Lu, K., Rohrer, F., Zhang, Y., and Brown, S. S.: A broadband cavity enhanced absorption spectrometer for aircraft measurements of glyoxal, methylglyoxal, nitrous acid, nitrogen dioxide, and water vapor, *Atmos. Meas. Tech.*, 9, 423-440, doi:10.5194/amt-9-423-2016, 2016.

Nakayama, T., Ide, T., Taketani, F., Kawai, M., Takahashi, K., and Matsumi, Y.: Nighttime measurements of ambient N_2O_5, NO_2, NO and O_3 in a sub-urban area, Toyokawa, Japan, *Atmos. Environ.*, 42, 1995-2006, doi:10.1016/j.atmosenv.2007.12.001, 2008.

Ng, N. L., Brown, S. S., Archibald, A. T., Atlas, E., Cohen, R. C., Crowley, J. N., Day, D. A., Donahue, N. M., Fry, J. L., Fuchs, H., Griffin, R. J., Guzman, M. I., Herrmann, H., Hodzic, A., Iinuma, Y., Jimenez, J. L., Kiendler-Scharr, A., Lee, B. H., Luecken, D. J., Mao, J., McLaren, R., Mutzel, A., Osthoff, H. D., Ouyang, B., Picquet-Varrault, B., Platt, U., Pye, H. O. T., Rudich, Y., Schwantes, R. H., Shiraiwa, M., Stutz, J., Thornton, J. A., Tilgner, A., Williams, B. J., and Zaveri, R. A.: Nitrate radicals and biogenic volatile organic compounds: oxidation, mechanisms, and organic aerosol, *Atmos. Chem. Phys.*, 17, 2103-2162, doi:10.5194/acp-17-2103-2017, 2017.

Noxon, J. F., Norton, R. B., and Marovich, E.: NO_3 in the troposphere, *Geophys. Res. Lett.*, 7, 125-128, doi:10.1029/GL007i002p00125, 1980.

Odame-Ankrah, C. A., and Osthoff, H. D.: A compact diode laser cavity ring-down spectrometer for atmospheric measurements of NO_3 and N_2O_5 with automated zeroing and calibration, *Appl. Spectrosc.*, 65, 1260-1268, doi:10.1366/11-06384, 2011.

Osthoff, H. D., Sommariva, R., Baynard, T., Pettersson, A., Williams, E. J., Lerner, B. M., Roberts, J. M., Stark, H., Goldan, P. D., Kuster, W. C., Bates, T. S., Coffman, D., Ravishankara, A. R., and Brown, S. S.: Observation of daytime N_2O_5 in the marine boundary layer during New England Air Quality Study-Intercontinental Transport and Chemical Transformation 2004, *J. Geophys. Res. Atmos.*, 111, n/a-n/a, doi:10.1029/2006jd007593, 2006.

Osthoff, H. D., Roberts, J. M., Ravishankara, A. R., Williams, E. J., Lerner, B. M., Sommariva, R., Bates, T. S., Coffman, D., Quinn, P. K., Dibb, J. E., Stark, H., Burkholder, J. B., Talukdar, R. K., Meagher, J., Fehsenfeld, F. C., and Brown, S. S.: High levels of nitryl chloride in the polluted subtropical marine boundary layer, *Nat. Geosci.*, 1, 324-328, doi:10.1038/ngeo177, 2008.

Platt, U., Perner, D., Winer, A. M., Harris, G. W., and and Pitts, J. N. J.: Detection of NO_3 in the polluted troposphere by differential optical absorption, *Geophys. Res. Lett.*, 7, 89-92, 1980.

Prakash, N., Ramachandran, A., Varma, R., Chen, J., Mazzoleni, C., and Du, K.: Near-infrared incoherent broadband cavity enhanced absorption spectroscopy (NIR-IBBCEAS) for detection and quantification of natural gas components, *Analyst.*, 143, 3284-3291, doi:10.1039/c8an00819a, 2018.

Roberts, J. M., Osthoff, H. D., Brown, S. S., and Ravishankara, A. R.: N_2O_5 oxidizes chloride to Cl_2 in acidic atmospheric aerosol, *Science*, 321, 1059-1059, doi:10.1126/science.1158777, 2008.

Schuster, G., Labazan, I., and Crowley, J. N.: A cavity ring down/cavity enhanced absorption device for measurement of ambient NO_3 and N_2O_5, *Atmos. Meas. Tech.*, 2, 1-13, doi:10.5194/amt-2-1-2009, 2009.

Shardanand, and Rao, A. P.: Absolute Rayleigh scattering cross sections of gases and freons of stratospheric interest in the visible and ultraviolet regions, NASA Technical Note, 1977.

Sheps, L.: Absolute ultraviolet absorption spectrum of a Criegee intermediate CH_2OO, *J. Phys. Chem. Lett.*, 4, 4201-4205, doi:10.1021/jz402191w, 2013.

Simpson, W. R.: Continuous wave cavity ring-down spectroscopy applied toin situdetection of dinitrogen pentoxide (N_2O_5), *Rev. Sci. Instrum.*, 74, 3442-3452, doi:10.1063/1.1578705, 2003.

Sobanski, N., Schuladen, J., Schuster, G., Lelieveld, J., and Crowley, J. N.: A five-channel cavity ring-down spectrometer for the detection of NO_2, NO_3, N_2O_5, total peroxy nitrates and total alkyl nitrates, *Atmos. Meas. Tech.*, 9, 5103-5118, doi:10.5194/amt-9-5103-2016, 2016.

Sommariva, R., Pilling, M. J., Bloss, W. J., Heard, D. E., Lee, J. D., Fleming, Z. L., Monks, P. S., Plane, J. M. C., Saiz-Lopez, A., Ball, S. M., Bitter, M., Jones, R. L., Brough, N., Penkett, S. A., Hopkins, J. R., Lewis, A. C., and Read, K. A.: Night-time radical chemistry during the NAMBLEX campaign, *Atmos. Chem. Phys.*, 7, 587-598, doi:10.5194/acp-7-587-2007, 2007.

Stark, H., Lerner, B. M., Schmitt, R., Jakoubek, R., Williams, E. J., Ryerson, T. B., Sueper, D. T., Parrish, D. D., and Fehsenfeld, F. C.: Atmospheric in situ measurement of nitrate radical (NO_3) and other photolysis rates using spectroradiometry and filter radiometry, *J. Geophys. Res. Atmos.*, 112, doi:10.1029/2006jd007578, 2007.

Stutz, J. A. B. A. R. G. A.: Vertical profiles of NO_3, N_2O_5, O_3, and NO_xin the nocturnal boundary layer: 1. Observations during the Texas Air Quality Study 2000, *J. Geophys. Res. Atmos.*, 109, doi:10.1029/2003jd004209, 2004.

Suhail, K., George, M., Chandran, S., Varma, R., Venables, D. S., Wang, M., and Chen, J.: Open path incoherent broadband cavity-enhanced measurements of NO_3 radical and aerosol extinction in the North China Plain, *Spectrochim. Acta A Mol. Biomol. Spectrosc.*, 208, 24-31, doi:10.1016/j.saa.2018.09.023, 2019.

Thalman, R., and Volkamer, R.: Inherent calibration of a blue LED-CE-DOAS instrument to measure iodine oxide, glyoxal, methyl glyoxal, nitrogen dioxide, water vapour and aerosol extinction in open cavity mode, *Atmos. Meas. Tech.*, 3, 1797-1814, doi:10.5194/amt-3-1797-2010, 2010.

Thalman, R., and Volkamer, R.: Temperature dependent absorption cross-sections of O_2–O_2 collision pairs between 340 and 630 nm and at atmospherically relevant pressure, *Phys. Chem. Chem. Phys.*, 15, 15371, doi:10.1039/c3cp50968k, 2013.

Varma, R. M., Venables, D. S., Ruth, A. A., Heitmann, U., Schlosser, E., and Dixneuf, S.: Long optical cavities for open-path monitoring of atmospheric trace gases and aerosol extinction, *Appl. Opt.*, 48, B159-B171, doi:10.1364/ao.48.00b159, 2009.

Venables, D. S., Gherman, T., Orphal, J., Wenger, J. C., and Ruth, A. A.: High sensitivity in situ monitoring of NO_3 in an atmospheric simulation chamber using incoherent broadband cavity-enhanced absorption spectroscopy, *Environ. Sci. Technol.* , 40, 6758-6763, doi:10.1021/es061076j, 2006.

Vrekoussis, M., Kanakidou, M., Mihalopoulos, N., Crutzen, P. J., Lelieveld, J., Perner, D., Berresheim, H., and Baboukas, E.: Role of the NO_3 radicals in oxidation processes in the eastern Mediterranean troposphere during the MINOS campaign, *Atmos. Chem. Phys.*, 4, 169-182, doi:10.5194/acp-4-169-2004, 2004.

Wagner, N. L., Dubé, W. P., Washenfelder, R. A., Young, C. J., Pollack, I. B., Ryerson, T. B., and Brown, S. S.: Diode laser-based cavity ring-down instrument for NO_3, N_2O_5, NO, NO_2 and O_3 from aircraft, *Atmos. Meas. Tech.*, 4, 1227-1240, doi:10.5194/amt-4-1227-2011, 2011.

Wang, D., Hu, R. Z., Xie, P. H., Liu, J. G., Liu, W. Q., Qin, M., Ling, L. Y., Zeng, Y., Chen, H., Xing, X. B., Zhu, G. L., Wu, J., Duan, J., Lu, X., and Shen, L. L.: Diode laser cavity ring-down spectroscopy for in situ measurement of NO_3 radical in ambient air, *J. Quant. Spectrosc. Radiat. Transf.*, 166, 23-29, doi:10.1016/j.jqsrt.2015.07.005, 2015.

Wang, H., Chen, J., and Lu, K.: Development of a portable cavity-enhanced absorption spectrometer for the measurement of ambient NO_3 and N_2O_5: experimental setup, lab characterizations, and field applications in a poll, *Atmos. Meas. Tech.*, 10, 1465-1479, doi:10.5194/amt-10-1465-2017, 2017.

Wang, H., and Lu, K.: Monitoring ambient nitrate radical by open-path cavity-enhanced absorption spectroscopy, *Anal. Chem.*, 91, 10687-10693, doi:10.1021/acs.analchem.9b01971, 2019.

Wang, H., Chen, X., Lu, K., Hu, R., Li, Z., Wang, H., Ma, X., Yang, X., Chen, S., Dong, H., Liu, Y., Fang, X., Zeng, L., Hu, M., and Zhang, Y.: NO_3 and N_2O_5 chemistry at a suburban site during the EXPLORE-YRD campaign in 2018, *Atmos. Environ.*, 224, 117180, doi:10.1016/j.atmosenv.2019.117180, 2020.

Wang, M., Varma, R., Venables, D. S., Zhou, W., and Chen, J.: A demonstration of broadband cavity-enhanced absorption spectroscopy at deep-ultraviolet wavelengths: Application to sensitive real-time detection of the aromatic pollutants benzene, toluene, and xylene, *Anal. Chem.*, 94, 4286-4293, doi:10.1021/acs.analchem.1c04940, 2022.

Wang, S., Shi, C., Zhou, B., Zhao, H., Wang, Z., Yang, S., and Chen, L.: Observation of NO_3 radicals over Shanghai, China, Atmos. Environ., 70, 401-409, doi:10.1016/j.atmosenv.2013.01.022, 2013.

Wang, X., Wang, T., Yan, C., Tham, Y. J., Xue, L., Xu, Z., and Zha, Q.: Large daytime signals of N_2O_5 and NO_3 inferred at 62 amu in a TD-CIMS: chemical interference or a real atmospheric phenomenon?, *Atmos. Meas. Tech.*, 7, 1-12, doi:10.5194/amt-7-1-2014, 2014.

Washenfelder, R. A., Langford, A. O., Fuchs, H., and Brown, S. S.: Measurement of glyoxal using an incoherent broadband cavity enhanced absorption spectrometer, *Atmos. Chem. Phys.*, 8, 7779-7793, doi:10.5194/acp-8-7779-2008, 2008.

Werle, P., MuCke, R., and Slemr, F.: The limits of signal averaging in atmospheric trace-gas monitoring by tunable diode-laser absorption spectroscopy (TDLAS), *Appl. Phys. B-Photo.*, 57, 131-139, doi:10.1007/bf00425997, 1993.

Winer, A. M., Atkinson, R., and Pitts, J. N.: Gaseous nitrate radical: Possible nighttime atmospheric sink for biogenic organic compounds, *Science*, 224, 156-159, doi:10.1126/science.224.4645.156, 1984.

Wood, E. C., Wooldridge, P. J., Freese, J. H., Albrecht, T., and Cohen, R. C.: Prototype for in situ detection of atmospheric NO_3 and N_2O_5 via laser-induced fluorescence, *Environ. Sci. Technol.* , 37, 5732-5738, doi:10.1021/es034507w, 2003.

Wu, H., Chen, J., Liu, A. W., Hu, S. M., and Zhang, J. S.: Cavity ring-down spectroscopy measurements of ambient NO_3 and N_2O_5 dagger, *Chinese J. Chem. Phys.*, 33, 1-7, doi:10.1063/1674-0068/cjcp1910173, 2020.

Wu, T., Coeur-Tourneur, C., Dhont, G., Cassez, A., Fertein, E., He, X., and Chen, W.: Simultaneous monitoring of temporal profiles of NO_3, NO_2 and O_3 by incoherent broadband cavity enhanced absorption spectroscopy for atmospheric applications, *J. Quant. Spectrosc. Radiat. Transf.*, 133, 199-205, doi:10.1016/j.jqsrt.2013.08.002, 2014.

Yokelson, R. J., Burkholder, J. B., Fox, R. W., Talukdar, R. K., and Ravishankara, A. R.: Temperature dependence of the NO_3 absorption spectrum, *J. Phys. Chem.*, 98, 13144-13150, doi:10.1021/j100101a009, 1994.

Young, I. A. K., Murray, C., Blaum, C. M., Cox, R. A., Jones, R. L., and Pope, F. D.: Temperature dependent structured absorption spectra of molecular chlorine, *Phys. Chem. Chem. Phys.*, 13, 15318, doi:10.1039/c1cp21337g, 2011.

Young, I. A. K., Jones, R. L., and Pope, F. D.: The UV and visible spectra of chlorine peroxide: Constraining the atmospheric photolysis rate, *Geophys. Res. Lett.*, 41, 1781-1788, doi:10.1002/2013gl058626, 2014.

Zhou, W., Zhao, J., Ouyang, B., Mehra, A., Xu, W., Wang, Y., Bannan, T. J., Worrall, S. D., Priestley, M., Bacak, A., Chen, Q., Xie, C., Wang, Q., Wang, J., Du, W., Zhang, Y., Ge, X., Ye, P., Lee, J. D., Fu, P., Wang, Z., Worsnop, D., Jones, R., Percival, C. J., Coe, H., and Sun, Y.: Production of N_2O_5 and $ClNO_2$ in summer in urban Beijing, China, *Atmos. Chem. Phys.*, 18, 11581-11597, doi:10.5194/acp-18-11581-2018, 2018.

760 **Table 1:** Comparison of BBCEAS performances for NO_3 measurement.

Reference	Eff. light path length (mirror displacement)	Reflectivity (max. performance)	Detection limit (time resolution)	Accuracy	Application[a]
Ball et al. (2004)	N/A	99.9965 % @ 670 nm	2.5 pptv (1σ, 516 seconds)	N/A	Laboratory
Venables et al. (2006)	2 km (4.5 m) @ 665 nm	99.775 % @ 665 nm	4 pptv (N/A,60 seconds)	14 %	Laboratory
Langridge et al. (2008)	11.8 km (1.1 m) @ 660 nm	99.9913 % @ 660 nm	0.25 pptv (1σ ,10 seconds)	N/A	M, France
Varma et al. (2009)[b,c,d]	33.5 km (8.6 m) @ 665 nm	99.98 % @ 662 nm	1 pptv (1σ ,5 seconds)	16 %	M, Ireland
Kennedy et al. (2011)	10 km (0.94 m)	N/A	1.1 pptv (1σ, 1 second)	11 %	M, UK
Wu et al. (2014)	22 km (2 m)	99.991 % @ [638, 672 nm]	7.9 pptv (N/A, 60 seconds)	12 %	Laboratory
Wang et al. (2017)[d]	6.13 km (0.33 m) @ 662 nm	99.9936 % @ 662 nm	2.4 pptv (1σ, 1 second)	19 %	U, China
Suhail et al. (2019)[b]	6.5 km (4.5 m) @ 660 nm	99.95 % @ 660 nm	36 pptv (N/A, 600 seconds)	N/A	SU, China
Wang and Lu (2019)[b]	5.1 km (0.84 m) @ 665 nm	99.985 % @ 662 nm	3.0 pptv (2σ, 30 seconds)	11–15 %	U, China
Fouqueau et al. (2020)	3.15 km (0.82 m) @ 662 nm	99.974 % @ 662 nm	6 pptv (N/A, 10 seconds)	9 %	Laboratory
This work	101.5 km (0.52 m) @ 662 nm	99.9995 % @ 662 nm	1.41 pptv (1σ, 1 second)	10.8 %	M, Arctic

a: U : urban region, SU : suburban region, M : marine region

b: systems with open cavity

c : ambient NO_3 was well below the detection limit through the whole measurement period

d: average values of reflectivity are noted instead of maximum values

765

https://doi.org/10.5194/egusphere-2022-145
Preprint. Discussion started: 11 April 2022

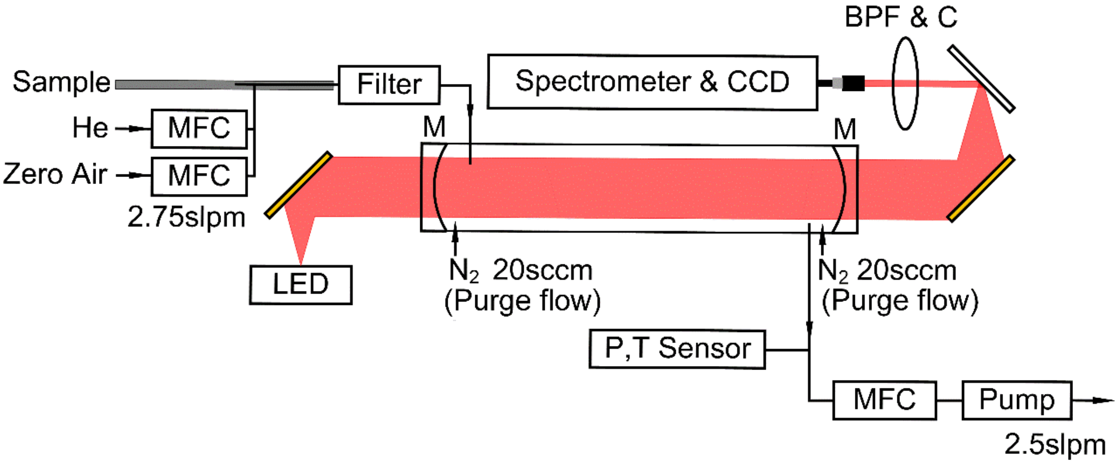

Figure 1: Schematic of the NO_3 BBCEAS system with light path (shaded in red) and gas flows (black arrows). High-reflection mirrors (M), band-pass filter (BPF), fiber collimator (C), mass flow controllers (MFC), and sensors of precision pressure transducer (P) and thermocouple (T) are marked.

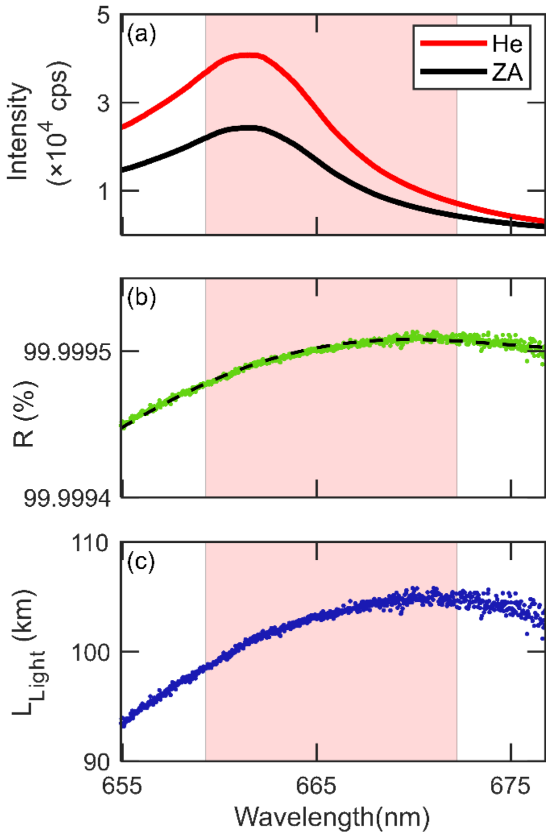

770 **Figure 2:** Cavity characteristics of 1 minute averaged **(a)** transmitted light intensities of zero air (ZA) and He, **(b)** mirrors reflectivity, R (dashed black line is fitted with fourth-order polynomial) and **(c)** effective light path length, L_{Light}. Shaded area in light red represents fitted range for the number density retrieval.

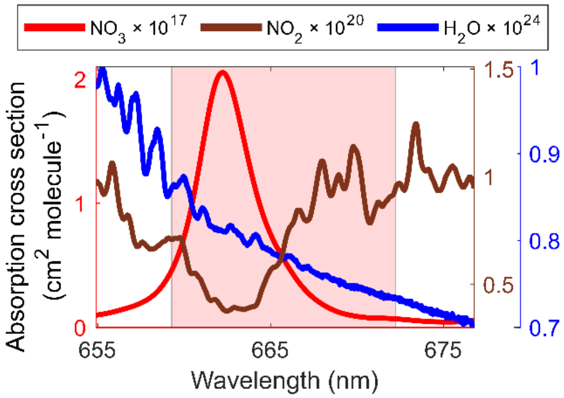

Figure 3: Used absorption cross-sections of NO_3, NO_2, and H_2O and fitting range (shaded in light red) for number density retrievals.

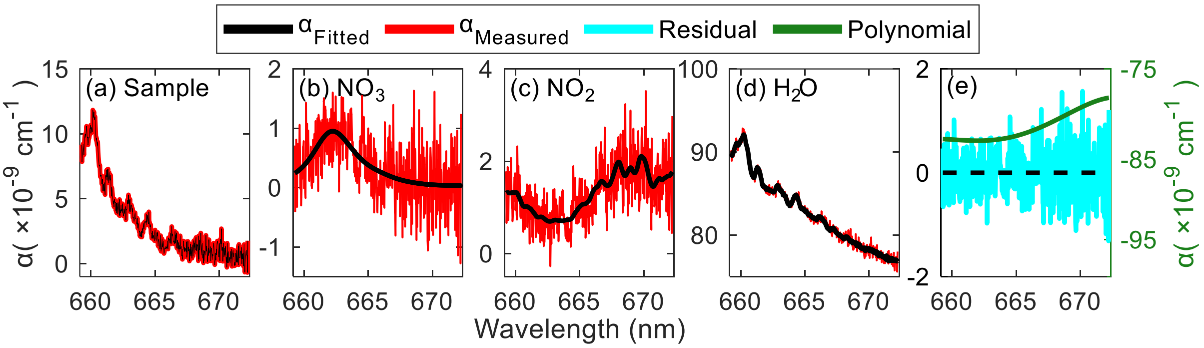

Figure 4: Spectral fitting example (2 seconds average) of ambient measured (red) and fitted (black) **(a)** total extinction, **(b)** NO_3, **(c)** NO_2, **(d)** H_2O and **(e)** polynomial (green) with residual (cyan), respectively. Data was acquired on August 26th, 2021 (UTC) from shipborne measurement on open ocean in Arctic region.

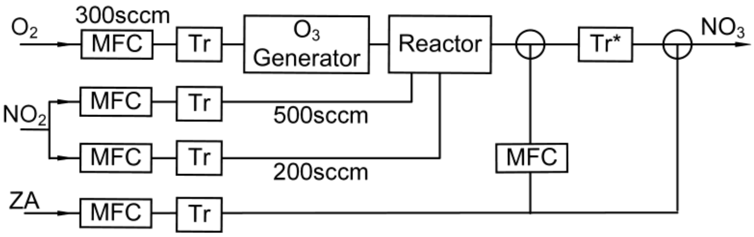

Figure 5: Schematic diagram of NO_3 generation system with flow paths (arrows). Dry ice cold trap for H_2O removal (Tr) and for sample collection (Tr*) are also shown.

https://doi.org/10.5194/egusphere-2022-145
Preprint. Discussion started: 11 April 2022

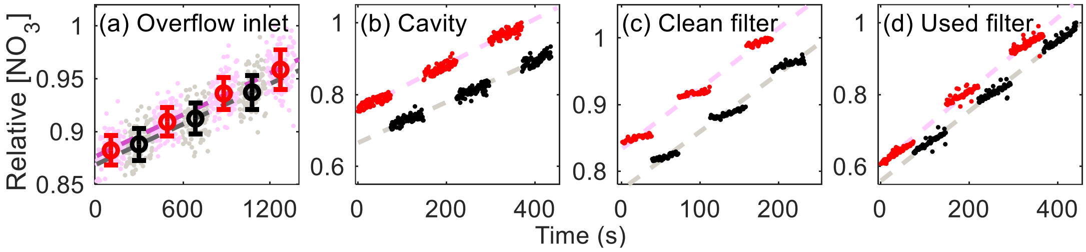

Figure 6: Relative NO$_3$ concentrations with (black) or without (red) test sections in **(a)** overflow inlet (averages as circle and 1σ as error bars), **(b)** cavity, **(c)** clean and **(d)** used filter (aerosol loading of 1,010 µg·cm^{-3}). Light red and gray dashed lines represent concentration drifts inferred from linear interpolation of each condition.

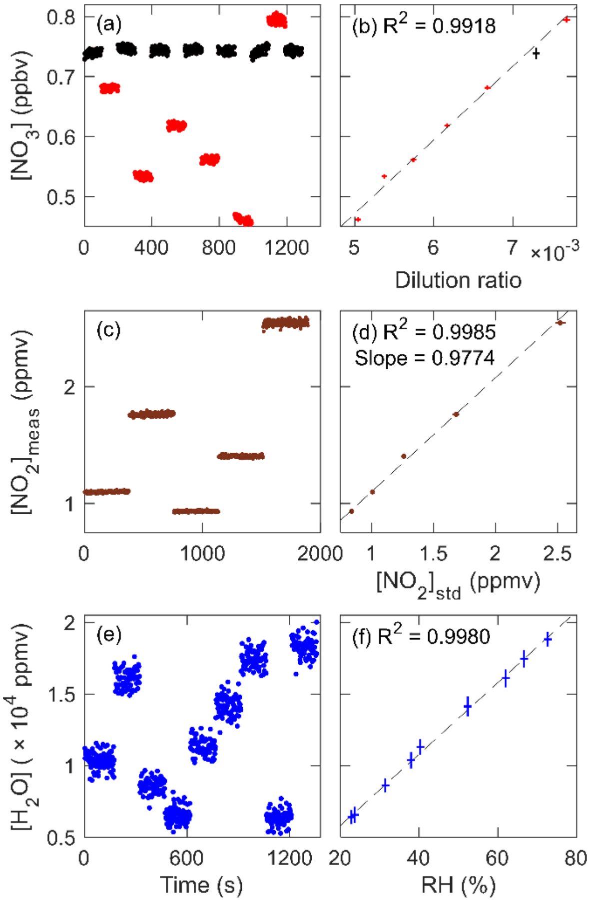

Figure 7: NO$_3$ **(a, b)**, NO$_2$ **(c, d)**, and H$_2$O **(e, f)** mixing ratios with elapsed times and other independent abundance evaluators in standard addition experiments. For NO$_3$, correction of the steady drift in NO$_3$ source bath was applied by linear interpolation of data with frequent injections of constant dilution condition (black). Error bars in (b, d, and f) represent 1σ variabilities for 2 seconds integration data (vertical) and uncertainty of evaluators (horizontal), while dashed lines show linear correlations.

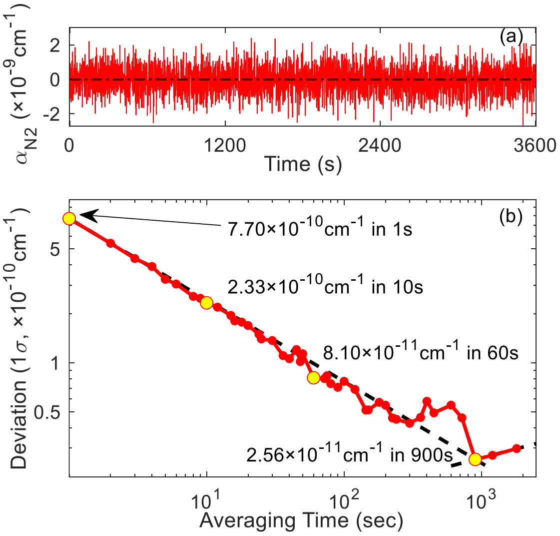

Figure 8: (a) Time series of light extinction for 1 hour of N_2 injection (1 second integration) and its **(b)** Allan deviations (1σ) for the single pixel at 662 nm. Yellow circles represent deviations for 1, 10, 60 and 900 seconds, respectively, and dashed line indicates theoretical limit representing white noise (slope : -0.5)

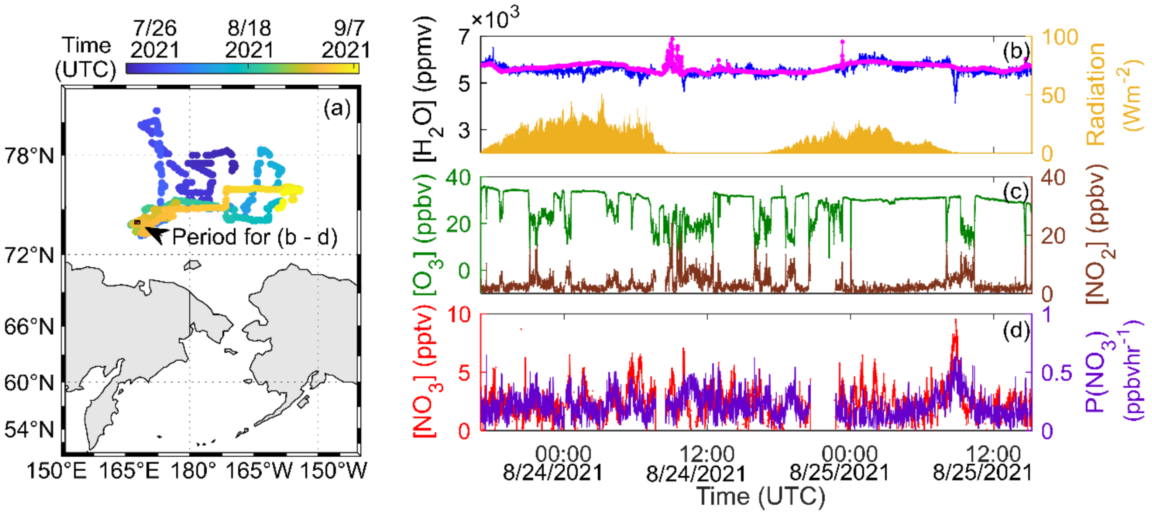

Figure 9: (a) A map with cruise track of R/V *Araon* and **(b–d)** representative time series of 1-minute averaged H_2O (measured by our instrument on compass deck in blue and a Vaisala instrument on mainmast in pink), radiation, NO_2, O_3 and NO_3 with calculated production rate of NO_3 for 23 August at 17:00 – 25 August at 15:10 in 2021 (UTC) on the open ocean in Arctic region.